Desalination and Water Treatment
www.deswater.com

doi: 10.5004/dwt.2023.29501

292 (2023) 108–121
April

Ipomoea batatas vine-derived activated carbon: a utility and efficient adsorbent for removing Cr(VI) from aqueous solution

Jiahui Deng[a,c], Min Liu[a], Xu Gong[a], Haisheng Tao[a,b,*]

[a]*Collaborative Innovation Center of Recovery and Reconstruction of Degraded Ecosystem in Wanjiang Basin Co-founded by Anhui Province and Ministry of Education, Anhui Provincial Engineering Laboratory of Water and Soil Pollution Control and Remediation, School of Ecology and Environment, Anhui Normal University, Wuhu 241000, China, emails: taohaish@mail.ahnu.edu.cn (H.S. Tao), 1792958536@qq.com (J.H. Deng), 3253350063@qq.com (M. Liu), 2465181251@qq.com (X. Gong)*
[b]*Anhui Laboratory of Molecule-Based Materials, College of Chemistry and Materials Science, Anhui Normal University, Wuhu 241000, China*
[c]*Chizhou University, Chizhou 247000, China*

Received 18 August 2022; Accepted 23 March 2023

ABSTRACT

In this work, an efficient activated carbon derived from *Ipomoea batatas* vine was used to remove hexavalent chromium (Cr(VI)) from wastewater. A series of characterization results of the activated carbon revealed that one of the prepared activated carbon (prepared at 800°C) had a high specific surface area (1,508.4 m^2/g), rich functional groups, etc. Batch adsorption experiments were carried out to explore the adsorption effect and mechanism of AC-800 on Cr(VI) in aqueous solution. The adsorption kinetic and isotherms experiment results fitted well with the pseudo-second-order kinetic model and the Langmuir isotherm model, respectively, which indicated that the adsorption of Cr(VI) by AC-800 was mainly by surface chemical complexation reaction, and the maximum adsorption capacity was 362.3 mg/g (in optimized condition). The efficiency of Cr(VI) removal was significantly affected by the initial pH of the solution. And, AC-800 showed good reusability, and the removal efficiency of Cr(VI) was still over 70% after four cycles. Overall, the activated carbon derived from discarded *Ipomoea batatas* vine could be considered an efficient adsorbent for Cr(VI) removal from aqueous solution.

Keywords: Activated carbon; *Ipomoea batatas* vine; Chromium; Removal; Mechanism

1. Introduction

The water pollution crisis has become a global issue, and one of the main factors of this crisis is heavy metal pollution due to its toxic, persistent and bio-accumulative nature [1,2]. Chromium (Cr) is widely used in electrical equipment and leather tanning and other industrial processes, but a large amount of wastewater containing Cr has caused extensive and serious harm to the environment and human health [3–5]. It is worth mentioning that the toxicity of (Cr(VI)) is much higher than that of trivalent chromium (Cr(III)) due to its oxidative, cancerogenic and corrosive properties [6]. Even though plenty of strict laws have been passed by governments to control the concentration of Cr in drinking water (such as <0.1 mg/L, U.S. Environmental Protection Agency) [5], a large amount of wastewater containing Cr(VI) are still being produced and urgently needed to treat with an efficient method [7]. It is urgent to explore a cost-efficient and environment-friendly method to remove Cr(VI) in wastewater.

A variety of technologies have been developed to remove Cr(VI) in wastewater, such as chemical precipitation,

* Corresponding author.

membrane filtration, ion exchange, and adsorption [8–11]. Compared with other methods, adsorption has attracted much attention due to its cost-effectiveness and environmental friendliness [12]. The high-efficient and low-cost adsorbent is the most fascinating in the adsorption process. Therefore, activated carbon derived from biomass has drawn wide attention because of its low cost, vast resource, and excellent potential to improve the value-added of biomass [13].

Many kinds of waste biomass are used as activated carbon, and show good adsorption effect [14–17]. However, an activated carbon prepared from *Ipomoea batatas* vine and used for the adsorption of Cr(VI) in water has not been explored. Even, many studies have shown that *Ipomoea batatas* vine is rich in crude fiber and lignin, which are extremely suitable for preparing activated carbon [18–21]. Besides, *Ipomoea batatas* are one of the most widely cultivated crops in the world, which could produce a large amount of waste vine every year [22–24]. In this work, a novel method has been explored to enhance the utility value of discarded *Ipomoea batatas* vine.

This work aims at investigating the adsorption ability of the *Ipomoea batatas* vine-derived activated carbon to remove Cr(VI) from aqueous solution. During the study, (a) the influence of adsorption process parameters was evaluated by batch experiments and (b) the mechanism of Cr(VI) adsorption was explored by comparing the characterizations and the adsorption performance of the different adsorbents.

2. Experimental set-up

2.1. Materials and reagents

Ipomoea batatas vines were collected from cropland (Anhui, China) and used as raw materials. Potassium hydroxide (AR grade) and hydrochloric acid (AR grade) were purchased from Sinopharm Chemical Reagent Co., Ltd., (Shanghai, China). Potassium dichromate (AR grade) was purchased from Shanghai Lingfeng Chemical Reagent Co., Ltd., (Shanghai, China). The pure water used in the whole experiment was obtained from the AquaPro Water Purification System (≥18.2 MΩ cm, 25°C). The real sample of river water was obtained from the Wuhu section of the Yangtze River, China. Several kinds of Cr(VI) stock solution (1,000 mg/L) were prepared by dissolving a certain amount of potassium dichromate in each water, and then stored at room temperature for further use. The solutions used in each experiment were obtained by diluting the standard reserve solution.

2.2. Preparation of Ipomoea batatas vines-derived activated carbons

Before the physico-chemical activation process, the *Ipomoea batatas* vines were washed with pure water to get rid of the adhered to impurities and dried in an oven for 24 h, followed by crushed and sieved to obtain an *Ipomoea batatas* powder for further manipulation. Subsequently, the *Ipomoea batatas* vines powder was carbonized to pristine biochar (BC) in a muffle furnace at 500°C for 2 h with a heating rate of 5°C/min. During the process of activation, BC and KOH were first mixed in water at a mass ratio of 1:3 [25], and then, the mixture was dried in an oven at 80°C for thoroughly stirred. The gained mixture was calcined in a muffle furnace at 600, 700, and 800°C for 90 min under nitrogen protection with a heating rate of 5°C/min, respectively. Finally, the obtained substances were washed with diluted hydrochloric acid and repeatedly washed with pure water to neutralize, then dried in an oven at 80°C for 24 h. The obtained activated carbons at different temperatures were labeled as AC-600, AC-700, and AC-800. The yield (Y) of AC-600, AC-700, and AC-800 was calculated by the following formulate:

$$Y(\%) = \frac{m_2}{m_1} \times 100 \tag{1}$$

where m_1 is the quality of dried *Ipomoea batatas* vines and m_2 is the quality of the prepared activated carbon.

2.3. Characterization

2.3.1. pH_{pzc} determination

The pH_{pzc} (point of zero charge) of the prepared activated carbons were determined as follows: the dried samples were poured into NaCl solutions (50 mL, 0.1 M), in which the initial pH range is 1–12, agitated at 25°C for 48 h. Then, the solution was filtered and the final pH was detected.

2.3.2. Fourier-transform infrared spectroscopy analysis

The functional groups were analyzed on Fourier-transform infrared spectrometer (FTIR, Thermo Scientific Nicolet iS5, USA) with a wavenumber range from 400 to 4,000 cm^{-1}.

2.3.3. Morphology analysis and porosity properties

The surface morphology and elemental analysis of the activated carbon were observed using scanning electron microscopy (SEM, Quanta FEG 250, USA). The surface areas and porosity properties of the activated carbon were investigated using Micromeritics ASAP 2460 Version 2.02 (USA) at 77 K. The specific surface areas were calculated by the Brunauer–Emmett–Teller (BET) method, and the volume and diameter of the micropore were calculated by the Horvath–Kawazoe (HK) and Barrett–Joyner–Halenda (BJH) methods. The spectra of X-ray photoelectron spectroscopy (XPS) were obtained by using Thermo Scientific Nexsa (US) with mono Al Kα radiation at 1,486.6 eV.

2.4. Adsorption experiments

Batch adsorption experiments were performed to evaluate the performance of the activated carbons for removing Cr(VI) from the aqueous solution. In each batch adsorption experiment, the pH value of Cr(VI) solution was adjusted by 1 M NaOH or 1 M HCl solution. Each adsorbent was weighed and placed in a flask with the same specification containing 200 mL Cr(VI) solution. The flask was then shaken horizontally at 150 rpm for a specified time. Subsequently,

the mixture was filtration with quantitative filter paper, and the remained chromium concentration in the filtrate was determined using the UV-Vis spectrophotometer (UV-1800PC, Mapada, Shanghai, China) at the wavelength of 540 nm using the colorimetric method.

Batch adsorption experiments under different conditions were employed to evaluate the parameters affecting adsorption, which included the initial pH value of Cr(VI) solution ranging from 2 to 10 and the dosage of adsorbent 0.01–0.06 mg. In the adsorption kinetic experiments, various adsorbents were added to 100 mL Cr(VI) solution (200 mg/L, pH = 2) and shaken at 150 rpm. A sample (0.5 mL) was then taken at different time intervals to analyze by a spectrophotometer. The isothermal adsorption experiments were carried out in Cr(VI) solution (pH = 2) with concentrations ranging from 50 to 300 mg/L. The adsorption thermodynamic experiments were carried out in Cr(VI) solution (pH = 2) with a concentration of 200 mg/L at 15°C, 25°C, 35°C, and 45°C. Each adsorption experiment was performed twice, and the average value was reported. The removal percentage was calculated as following equations:

$$r = \frac{\left(C_0 - C_e\right)}{C_0} \times 100 \tag{2}$$

$$Q_e = \frac{\left(C_0 - C_e\right)}{m} \times V \tag{3}$$

$$Q_t = \frac{\left(C_0 - C_t\right)}{m} \times V \tag{4}$$

where C_0, C_e, and C_t (mg/L) represent the concentration of Cr(VI) in the solution at initial, adsorption equilibrium, and time t, respectively. r is the removal rate of Cr(VI). Q_e and Q_t are the capacities of adsorbent at adsorption equilibrium and time t, respectively. m presents the mass of AC-600, AC-700, and AC-800. V is the volume of the Cr(VI) solution.

2.5. Experimental data models

Adsorption isotherm models including the Langmuir isotherm, the Freundlich isotherm, and the Temkin isotherm were used to fit isothermal adsorption experimental data. The mathematical equations are as follows [26].

Langmuir isotherm:

$$\frac{C_e}{Q_e} = \frac{1}{Q_{\max} K_l} + \frac{C_e}{Q_{\max}} \tag{5}$$

Adsorption feasibility:

$$R_L = \frac{1}{\left(1 + \left(C_0 K_l\right)\right)} \tag{6}$$

Freundlich isotherm:

$$\ln Q_e = \ln K_f + \frac{1}{n}\left(\ln C_e\right) \tag{7}$$

Temkin isotherm:

$$Q_e = B \ln A + B \ln C_e \tag{8}$$

where $Q_{\max}$ is the maximum adsorption capacity of adsorbents for Cr(VI), which is theoretically calculated from the Langmuir isotherm model. K_l is the Langmuir constant. R_L is a dimensionless constant separation factor, which could indicate the nature of the Langmuir isotherm model. K_f represents the Freundlich constant, and n is the heterogeneity factor of the Freundlich isotherm model. A and B represent Temkin constants.

The adsorption kinetic model, which includes the pseudo-first-order kinetic model, the pseudo-second-order kinetic model, and the Weber–Morris's intraparticle diffusion model, were used to fit adsorption experiment data [27]:

Pseudo-first-order kinetic model:

$$\log\left(Q_e - Q_t\right) = \log Q_e - \left(\frac{k_1 t}{2.303}\right) \tag{9}$$

Pseudo-second-order kinetic model:

$$\frac{t}{Q_t} = \frac{1}{k_2\left(Q_e^2\right)} + \frac{t}{Q_e} \tag{10}$$

Weber–Morris's intraparticle diffusion model:

$$Q_t = k_3 t^{1/2} + C \tag{11}$$

where k_1, k_2, and k_3 are considered as rate constants of the pseudo-first-order, the pseudo-second-order kinetic model, and the Weber–Morris's intraparticle diffusion model. t represents the contact time.

The adsorption thermodynamics parameters of Cr(VI) were estimated by the following equations [28]:

Linear partition:

$$K_d = \frac{Q_e}{C_e} \tag{12}$$

Gibbs free energy:

$$\Delta G^\circ = -RT \ln K_d \tag{13}$$

Van't Hoff:

$$\ln K_d = \frac{\Delta S^\circ}{R} - \frac{\Delta H^\circ}{RT} \tag{14}$$

where R is the universal gas constant, and T is the temperature of the adsorption system. K_d is the partition coefficient. ΔS° and ΔH° are the enthalpy change and the entropy change, respectively, calculated from the slope and intercept of K_d vs. $1/T$.

2.6. Regeneration performance and practical application effect

The activated carbon was recycled 5 times to test its regeneration performance. During the regeneration

adsorption experiment, the used activated carbon was immersed in 1 M NaOH solution with stirring for 4 h, then filtered, washed with pure water three times, and dried at 80°C for 8 h. The recycled activated carbon was performed for the next adsorption experiment again. The 100 mg/L Cr(VI)-containing solutions prepared from the Yangtze River water were used to simulate real wastewater, and to evaluate the adsorption effect of Cr(VI) in real wastewater by the adsorbents.

3. Results and discussion

3.1. Characteristics and physico-chemical property of adsorbents

Scanning electron microscopy-energy-dispersive X-ray spectroscopy (SEM-EDS) was used to observe the morphology and measure the element content of the activated carbons, and SEM images and EDS data are displayed in Fig. 1. As Fig. 1a–c shows, the oxygen content on the surface of the activated carbon decreases gradually with the increase of pyrolysis temperature, and AC-800 has a smooth surface structure compared with others, which probably related to more organic matter is volatilized with the increase of pyrolysis temperature. The surface structure of AC-800 does not change significantly before and after adsorption, but the oxygen content on the surface of AC-800 increased obviously after adsorption, which could be related to the mass of $Cr_2O_7^{2-}$ and CrO_4^{2-} were adsorbed on the surface of the adsorbent via physical adsorption or chemical reaction (Fig. 1c and d). Meanwhile, the mapping image (Fig. S1) shows that Cr and O are evenly distributed on the surface of AC-800 after Cr(VI) adsorption. What's more, the Cr content is 9.69% (by weight) after Cr(VI) adsorption process, confirming Cr(VI) is efficiently adsorbed by AC-800.

The FTIR spectra of the activated carbons before and after adsorption are presented in Fig. 2. In the initial adsorbents' spectra, the peak exists at 3,427 cm^{-1} on behalf of the vibrations of C–OH bonds. Compared to the other two activated carbons, the peak at 1,585 and 1,116 cm^{-1} of AC-800 are enhanced, which respectively relates to arylalkyl ether ($–OCH_3$) and the C–O bond presented in ester and ether. This phenomenon could be because many long-chain organic matters and oxygen-containing functional groups volatilize and produce more C–H bonds during the pyrolysis process [29–32]. After adsorption, the broadband between 675 and 798 cm^{-1} weakens obviously (Fig. 2), which indicates the O–H and C–H bending presented in carboxylic acid and aromatic compound participated in the Cr(VI) adsorption process [33]. In addition, a significant decrease at the peak of C–H (569 cm^{-1}) and C–OH (3,427 cm^{-1}), which was due to the oxidation of carbon because of the reduction of Cr(VI) to

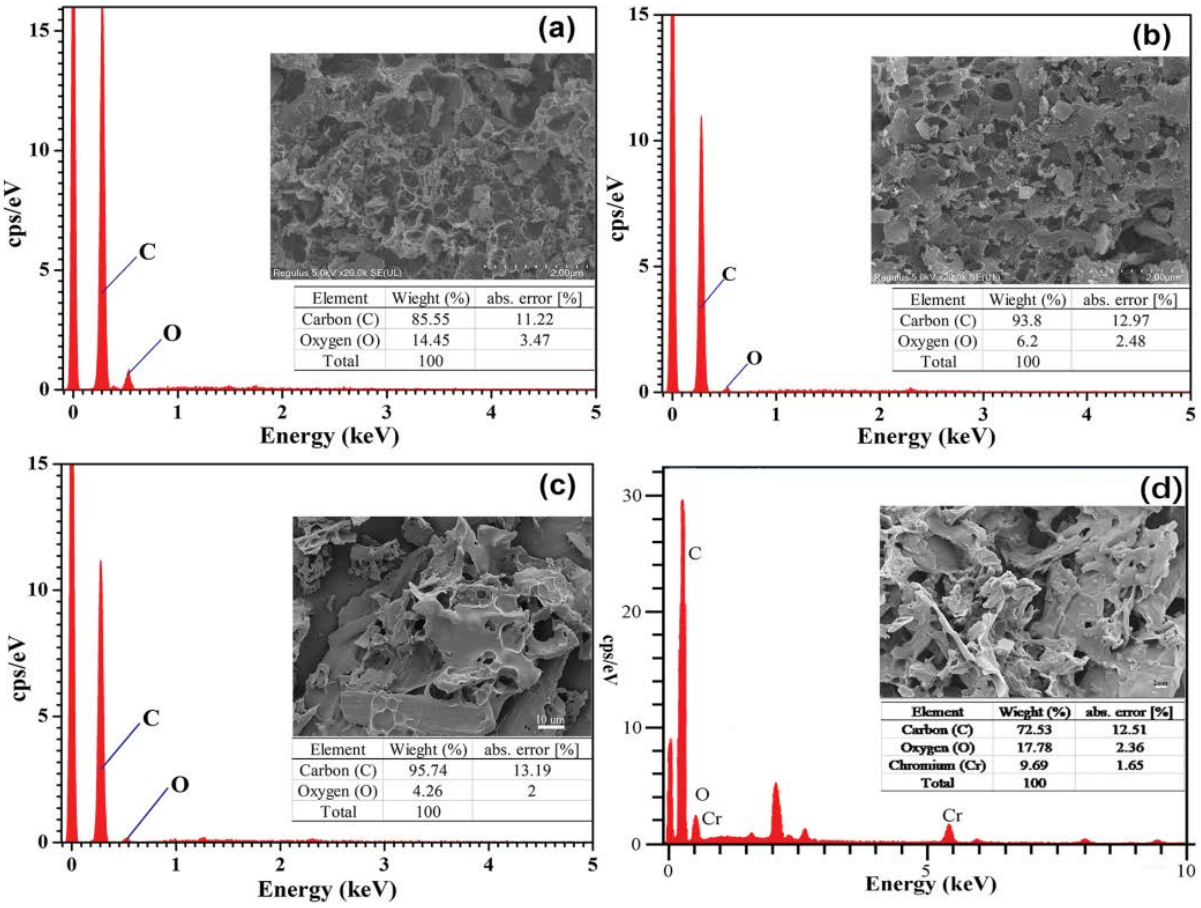

Fig. 1. Scanning electron microscopy-energy-dispersive X-ray spectroscopy images of (a) AC-600, (b) AC-700, (c) AC-800 before and (d) after Cr(VI) adsorption.

Cr(III) by AC-800 [34]. This phenomenon suggests that the removal efficiency of Cr(VI) by activated carbon is closely related to these functional groups.

As Fig. 3a shows, the nitrogen adsorption–desorption isotherms are type II and IV with H_4 hysteresis loop characteristics according to the International Union of Pure and Applied Chemistry (IUPAC) classification, which means the prepared activated carbons mainly have mesoporous and micropore structures. The pore-size distribution of the prepared activated carbons is shown in Fig. 3b, which further confirms that they have abundant micropores and mesopores. It is well known that micropores provide a huge amount of adsorption sites, while mesopores facilitate the transfer of heavy metal ions [35,36]. BET surface area is an important parameter of adsorbents, a larger specific surface area means more available adsorption sites. AC-800 possesses the largest specific surface area (S_{BET} = 1,508.4 m^2/g) and the smallest average pore size (2.18 nm) among the three activated carbons (Table 1), this is consistent with the observed result of SEM. As expected, the results of the nitrogen

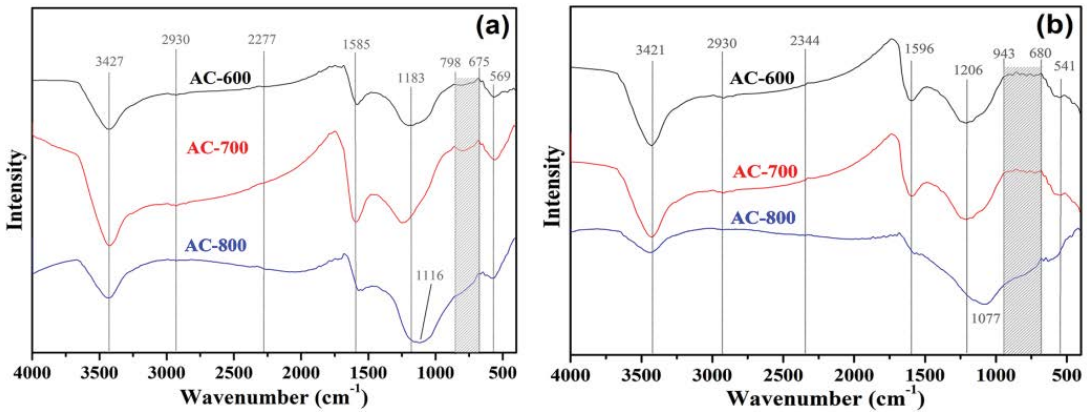

Fig. 2. Fourier-transform infrared spectroscopy of AC-600, AC-700, and AC-800 before (a) and after (b) adsorption.

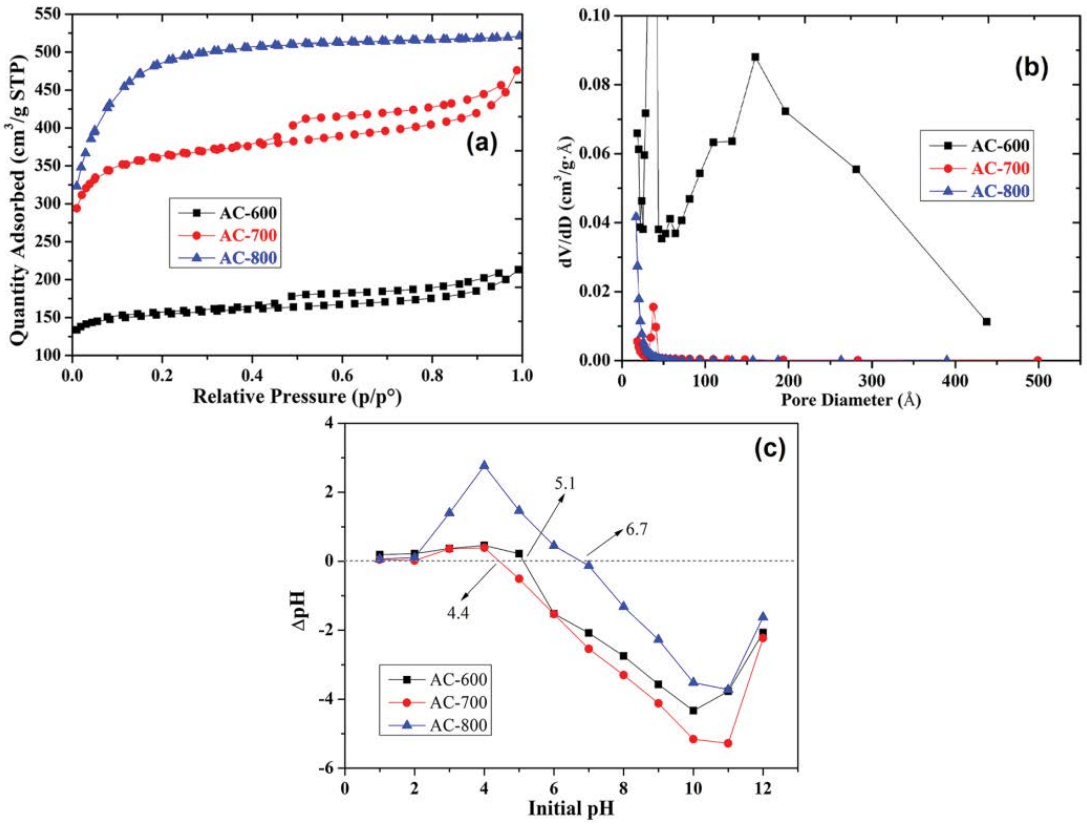

Fig. 3. Characterization of AC-600, AC-700, and AC-800, (a) N_2 adsorption–desorption isotherms, (b) pore-size distribution acquired by Barrett–Joyner–Halenda technique and (c) pH_{pzc}.

adsorption–desorption experiment prove that the increase of pyrolysis temperature is beneficial to the formation of mesopores and micropores, and simultaneously increases the specific surface area of the activated carbon. In addition, the pH_{pzc} for AC-800 is 6.7, which is higher than that of AC-600 and AC-700. This could be because of the evaporation of some organic matter in the process of pyrolysis. The higher value of pH_{pzc} means that the adsorbent can better adsorb Cr(VI) under acidic conditions by electrostatic adsorption [37].

3.2. Influence of initial pH

The initial pH value of the solution is an important factor affecting the adsorption of Cr(VI) by adsorbents. The removal rate for Cr(VI) of the prepared adsorbents decreases sharply with the increase of the solution pH in the range of 2–10. When the initial pH of the solution is 2, AC-800 does the best job of removing Cr(VI), and the removal rate is almost up to 100% (Fig. 4a). This phenomenon may be due to the content of several anionic forms of Cr(VI) in aqueous solution depends on solution pH, CrO_4^{2+} is dominant at pH > 6, while $Cr_2O_7^{2-}$ and $HCrO_4^{1-}$ are dominant Cr(VI) species at pH < 6. When pH < pH_{pzc}, the surface charge of AC-800 is positive, which favors the Cr(VI) adsorption. Moreover, the low pH value could increase the degree of protonation on the surface of the activated carbon, which would enhance the attraction between Cr(VI) and the activated carbon [38].

Table 1
Yields, physical and chemical properties of the prepared activated carbons

Parameter	AC-600	AC-700	AC-800
Yields, %	17.8	14.4	12.9
Brunauer–Emmett–Teller surface area, m^2/g	479.64	1,100.83	1,508.4
Total pore volume, cm^3/g	0.33	0.736	0.806
Average pore diameter (BJH), Å	52.746	49.991	21.829
Median pore width, Å	5.483	5.451	5.455
pH_{pzc}	5.1	4.4	6.7

Besides, the pH of the solution is obviously close to 7 after adsorption which means hydroxide ions are exhausted in the adsorption process (Fig. 4b). Further exploration reveals that the remained solution contains a large amount of Cr(III), which implied that hydrogen ions are consumed by the reduction reaction of Cr(VI) (Fig. S2). It is worth mentioning that the reduction efficiency of Cr(VI) by AC-800 is much better than that of other adsorbents.

3.3. Influence of adsorbents dose

Fig. 5 shows the influence of different dosages of the different adsorbents for Cr(VI) removal at the optimal pH of 2. The maximum removal rate for Cr(VI) using AC-800 is 99.75%. Compared with the other two adsorbents, AC-800 shows the largest adsorption capacity. As the mass of adsorbents increases, the removal rate of Cr(VI) gradually increases. Adversely, the adsorption capacity of Cr(VI) gradually decreases with the increase in adsorbents dosage, which indicate that a large number of adsorption sites are underutilized.

3.4. Adsorption kinetics

In order to further clarify the adsorption behavior of adsorbents, the adsorption kinetic experiment was carried out, and the results shown in Fig. 6. In the first 3 h, the adsorption amount of Cr(VI) on each adsorbent increases sharply and close to adsorption equilibrium, and the removal rate reach to 87.4% (Fig. 6a). This phenomenon indicates that the massive vacant adsorption sites at the initial adsorption phase are beneficial to Cr(VI) adsorption. The removal rate of Cr(VI) reduces with time, and adsorption equilibrium is reached after 6 h. This phenomenon may be because the readily available adsorption sites are gradually consumed and agglomeration of the adsorbents occurs in the adsorption process.

The experimental adsorption data were fitted with several kinetic models to gain an understanding of the adsorption behavior and the possible adsorption mechanism associated with the adsorption of Cr(VI). The model parameters for the three commonly kinetic models were calculated and shown in Table 2. The fitting results indicate that the

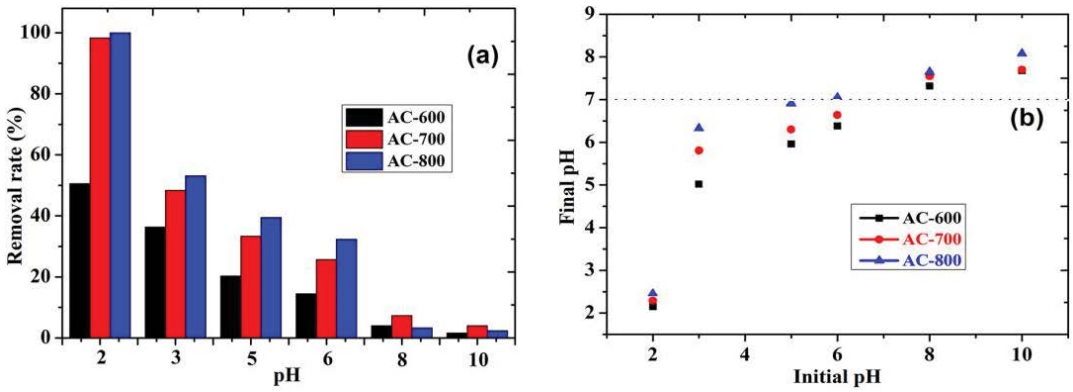

Fig. 4. (a) Removal rate of the activated carbons under different pH (25°C) and (b) the pH value of the solution after adsorption by the activated carbons.

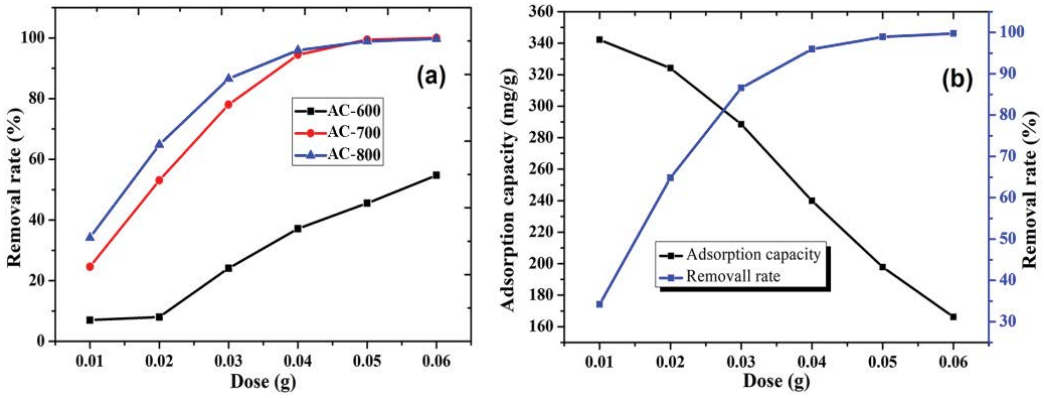

Fig. 5. (a) Adsorption capacity of AC-600, AC-700, AC-800 for Cr(VI) and (b) adsorption capacity and removal rate of AC-800 for Cr(VI), initial pH of 2, adsorption time of 24 h.

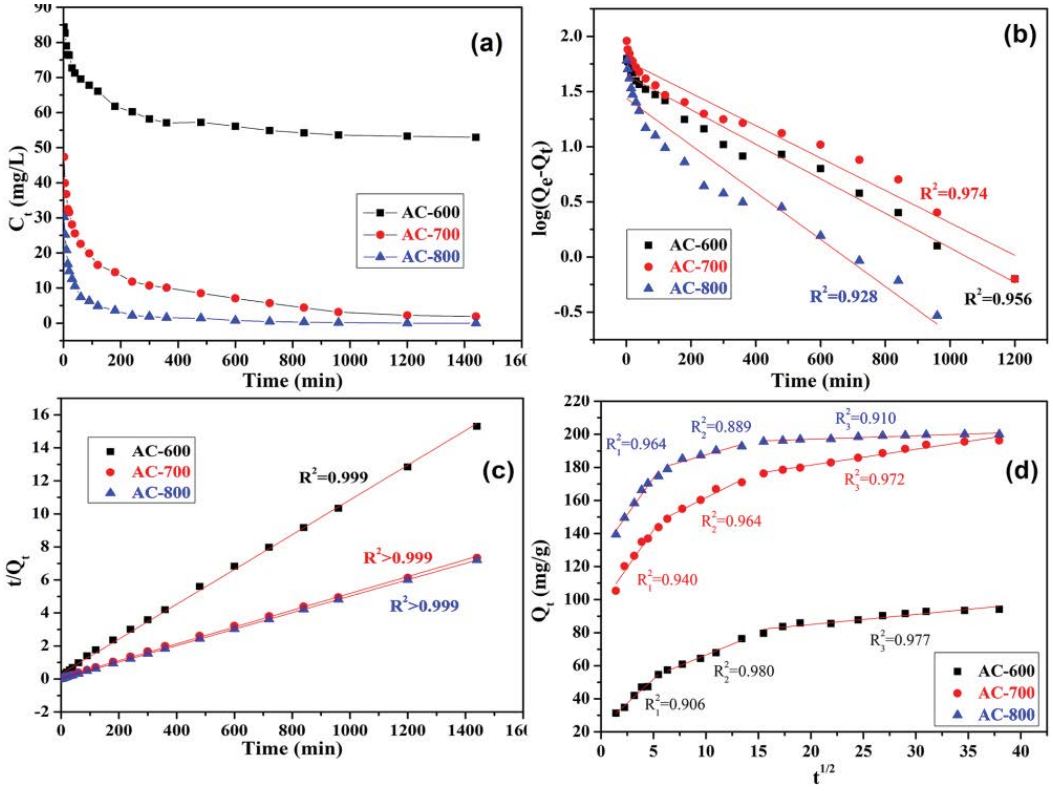

Fig. 6. Adsorption kinetic of Cr(VI) onto AC-600, AC-700, AC-800, and linear adjustments of the kinetic models (C_0 = 100 mg/L, T = 25°C ± 0.5°C, 150 rpm).

adsorption data fit best by the pseudo-second-order kinetic model with regression coefficients > 0.999, and no obvious difference is found between the experimental adsorption capacity (Q_{max}) and the theoretical adsorption capacity (Q_t) calculated by pseudo-second-order kinetic model, which means the pseudo-second-order kinetics model is the best suitable model to describe the adsorption behavior of each adsorbent ($R^2 > 0.999$). The results suggest that chemisorption might control the Cr(VI) adsorption process [39]. The high value of k_2 indicates the high removal efficiency of Cr(VI) by AC-800, because the huge specific surface area of AC-800 could provide abundant effective capture sites for Cr(VI).

In order to explore the diffusion mechanism and the rate-controlling step for Cr(VI) adsorption, Weber–Morris's intraparticle diffusion model was employed to fit the adsorption data, and the result is shown in Table 1. The adsorption data for Cr(VI) fit well with Weber–Morris's intraparticle diffusion model with regression coefficients >0.97, the result indicates that the intraparticle diffusion maybe exists in Cr(VI) adsorption process and affect the adsorption efficiency of each adsorbent [40]. As depicted in Fig. 6d, there are three stages for Cr(VI) adsorption process. The first stage is related to the transfer of Cr(VI) from the solution to the external surface of the adsorbents. The

Table 2
Kinetics parameters of Cr(VI) sorption by AC-600, AC-700, AC-800 at 25°C

Data type	Kinetics parameter	Adsorbents		
		AC-600	AC-700	AC-800
Experimental adsorption	Q_{max} (mg/g)	94.1	196.2	200
	k_1 (min^{-1})	0.0036	0.0034	0.0049
Pseudo-first-order kinetic model	Q_{cal} (mg/g)	148.93	318.60	138.23
	R^2	0.974	0.956	0.928
	k_2 (g/(mg·min))	0.00035	0.00030	0.0011
Pseudo-second-order kinetic model	Q_{cal} (mg/g)	95.0	196.1	200.4
	R^2	0.999	0.999	0.999
	k_3 (mg/(g·$min^{-1/2}$))	5.797	2.609	0.612
Weber–Morris's intraparticle diffusion model	C_1	22.9	96.7	129.1
	C_2	40.4	129.9	169.2
	C_3	72.7	162.1	192.8

second-stage is intraparticle diffusion, and the third stage presents the sorption equilibrium [41]. The intercept value (C_i) of the plots is related to the external diffusion resistance, and $C_1 < C_2 < C_3$ indicates the lowest adsorption resistance at the first stage, respectively.

3.5. Adsorption isotherms

Adsorption isotherms were employed to understand the partition of Cr(VI) between the solid and liquid phases under equilibrium conditions. The adsorption data for Cr(VI) sorption on adsorbents were analyzed by Langmuir, Freundlich, and Temkin isotherm. The fitting results and related parameters are shown in Table 3. As Fig. S3 shows, the adsorption capacity of the adsorbents increases remarkably with the increase of Cr(VI) initial concentration. The adsorption data fit with the Langmuir isotherm model (regression coefficients >0.991) best, implying that Cr(VI) adsorption is a monomolecular layer adsorption process [42]. The separation factor (K_l) is an essential factor for Langmuir isotherm, which can be used to verify the adsorption process, that is favorable ($0 < K_l < 1$), leaner ($K_l = 1$), or unfavorable ($K_l > 1$). The value of K_l is 1.605 for AC-800, implying the unfavourability of Cr(VI) adsorption. This phenomenon may due to the different surface structures of the three kinds of activated carbons. According to the Langmuir isotherm model, the maximum adsorption capacity of AC-800 is 362.3 mg/g at 25°C, which is much higher than that of the adsorbents reported in the other literature (Table 4).

3.6. Adsorption thermodynamic

The influence of temperature on the adsorption performance of Cr(VI) onto adsorbents was explored by carrying out experiments at different temperatures (15°C, 25°C, 35°C, and 45°C). Fig. 7 displays the relationship between the temperature and the Cr(VI) adsorption performance. The $\Delta G°$ values of AC-800 are all negative and decrease with the increase of temperature, which means the adsorption of Cr(VI) by AC-800 is spontaneous, and the degree of spontaneous increases with temperature. Besides, the positive

Table 3
Isotherm parameters of the equilibrium adsorption of Cr(VI) by AC-600, AC-700, AC-800 at 25°C

Isotherm model	Isotherm parameter	Adsorbents		
		AC-600	AC-700	AC-800
Langmuir isotherm	Q_{max} (mg/g)	124.5	311.6	362.3
	K_l	0.094	0.490	1.605
	R^2	0.991	0.997	0.999
Freundlich isotherm	K_f	73.900	201.001	229.770
	n	11.171	11.275	10.371
	R^2	0.916	0.990	0.970
Temkin isotherm	B	8.837	22.053	24.268
	A	2,563.058	8,970.957	33,576.48
	R^2	0.878	0.987	0.894

$\Delta H°$ and $\Delta S°$ values mean the Cr(VI) adsorption process is endothermic (Table 5) [50].

3.7. Regeneration and practical application

The regeneration is closely related to sustainability and an important economic factor for Cr(VI) treatment process. And the application of the activated carbons in complex water samples can verify their practical application value. As Fig. 8 shows, even after three cycles, the removal rate for Cr(VI) by AC-800 is still more than 70%. The reduction of adsorption capacity could be because of the depletion of functional groups or incomplete elution of Cr(VI). In addition, the activated carbons show excellent Cr(VI) removal effect even in simulated real wastewater (Fig. 8b). These results indicate that the activated carbons could be regenerated and reused for Cr(VI) removal.

3.8. Cr(VI) removal mechanism investigation

XPS has been employed to further analyze the surface chemical composition of fresh and used AC-800. As Fig. 9a

shows, the Cr peaks are observed at binding energy between 580.0 and 595.0 eV, the result proves Cr is adsorbed onto the adsorbents. The XPS analysis (Fig. 9b) shows the existence of Cr(III) on the surfaces of AC-800 with intensive peaks at 577.4 and 587.0 eV [51]. Here is the hypothesis that Cr(VI) is reduced to Cr(III) by AC-800 to form new products containing Cr(III) species (e.g., $Cr(OH)_3$), and these new products were precipitated on the surface of AC-800. Fig. 9c presents the XPS spectra of the activated carbon before and after adsorption in terms of C1s and O1s atomic orbitals. The activated carbon has a C1s peak deconvoluted into four peaks representing aromatic C–C/C=C (284.5 eV), aromatic C–C/C–H (285.0 eV), ketone C–O (286.3 eV), and carboxylic O–C=O (288.3 eV) [52,53]. After Cr(VI) adsorption, the single peak area at 285.0 eV and the O1s peak binding energy changes obviously, which is attributed to the oxidation of carbon because of the reduction of Cr(VI) to Cr(III) (Fig. 9c and d) [54–56]. This implies that the active functional groups contribute to Cr(VI) adsorption (e.g., complexation, reduction), which is consistent with the result of FTIR. Based on the above analysis, a possible model to describe the mechanism of Cr(VI) removal by AC-800. After the addition of AC-800, Cr(VI) was instantaneously adsorbed onto the surfaces of AC-800 by electrostatic attraction and complexation because of the positively charged surfaces, and hydroxyl groups of AC-800. Then, the surface bounded Cr(VI) could be reduced to Cr(III) by AC-800 directly, and deposited on the surface of AC-800.

The results of batch adsorption experiments indicating the pH of the solution determine the Cr(VI) adsorption efficiency onto the activated carbon. Under the acidic condition, the electronic attraction is the predominant factor for Cr(VI) adsorption, the positive surface charge of AC-800 could efficiently adsorb $Cr_2O_7^{2-}$ and $HCrO_4^-$ in solution. The effect of solution pH also confirms that part of Cr(VI) is reduced to Cr(III) through the electron donor on the surface of AC-800. Moreover, the huge S_{BET} of the activated carbon could provide abundantly available adsorption sites and reduction sites, which benefits the Cr(VI) adsorption and reduction. In addition, pseudo-second-order kinetic model implies the chemisorption control Cr(VI) adsorption process, and Weber–Morris's intraparticle diffusion model

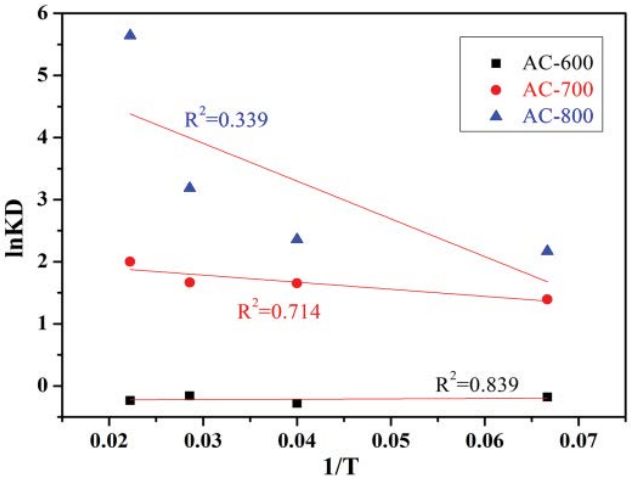

Fig. 7. Thermodynamic plot for Cr(VI) adsorption on adsorbents.

Table 4
Cr(VI) adsorption capacity of various adsorbents reported in the literatures

Adsorbent	Capacity (mg/g)	References
Corn stalk-based activated carbon	89.5	[7]
Chestnut oak shells activated carbon	33	[34]
Magnetic porous water hyacinth-derived biochar	202.61	[43]
Activated carbon derived from Bermuda grass	403.23	[44]
Eucalyptus sawdust activated carbon	45.88	[45]
Olive bagasse activated carbon	126.67	[46]
Coal gangue activated carbon	320.51	[47]
Natural diatomite-based carboxyl-rich carbon nanocomposite	142.857	[48]
Activated carbon prepared from longan seed	169.00	[49]
Ipomoea batatas vine-derived activated carbon	362.3	This study

Table 5
Thermodynamic parameters of Cr(VI) on the activated carbons at different temperatures

T (°C)	Δ*G*° (kJ/mol)			Δ*H*° (kJ/mol)			Δ*S*° (kJ/mol·K)		
	AC-600	AC-700	AC-800	AC-600	AC-700	AC-800	AC-600	AC-700	AC-800
15	22.43	–173.75	–270.54	–0.07	1.37	7.32	–0.03	0.26	0.69
25	58.12	–344.11	–490.35						
35	45.99	–486.66	–926.44						
45	88.34	–748.47	–2110.41						

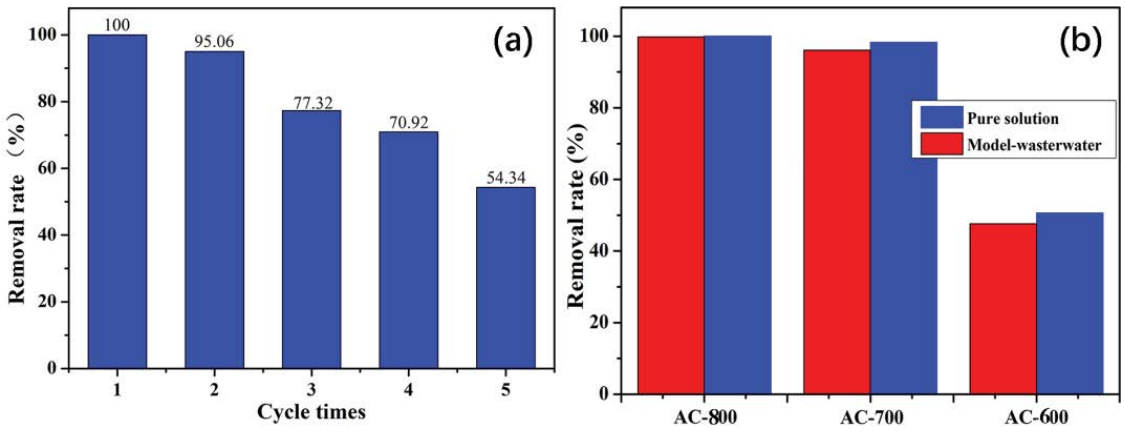

Fig. 8. The Cr(VI) removal efficiency of AC-800 after consecutive regeneration cycles (a), and removal rate of Cr(VI) in pure solution and model-wastewater (b).

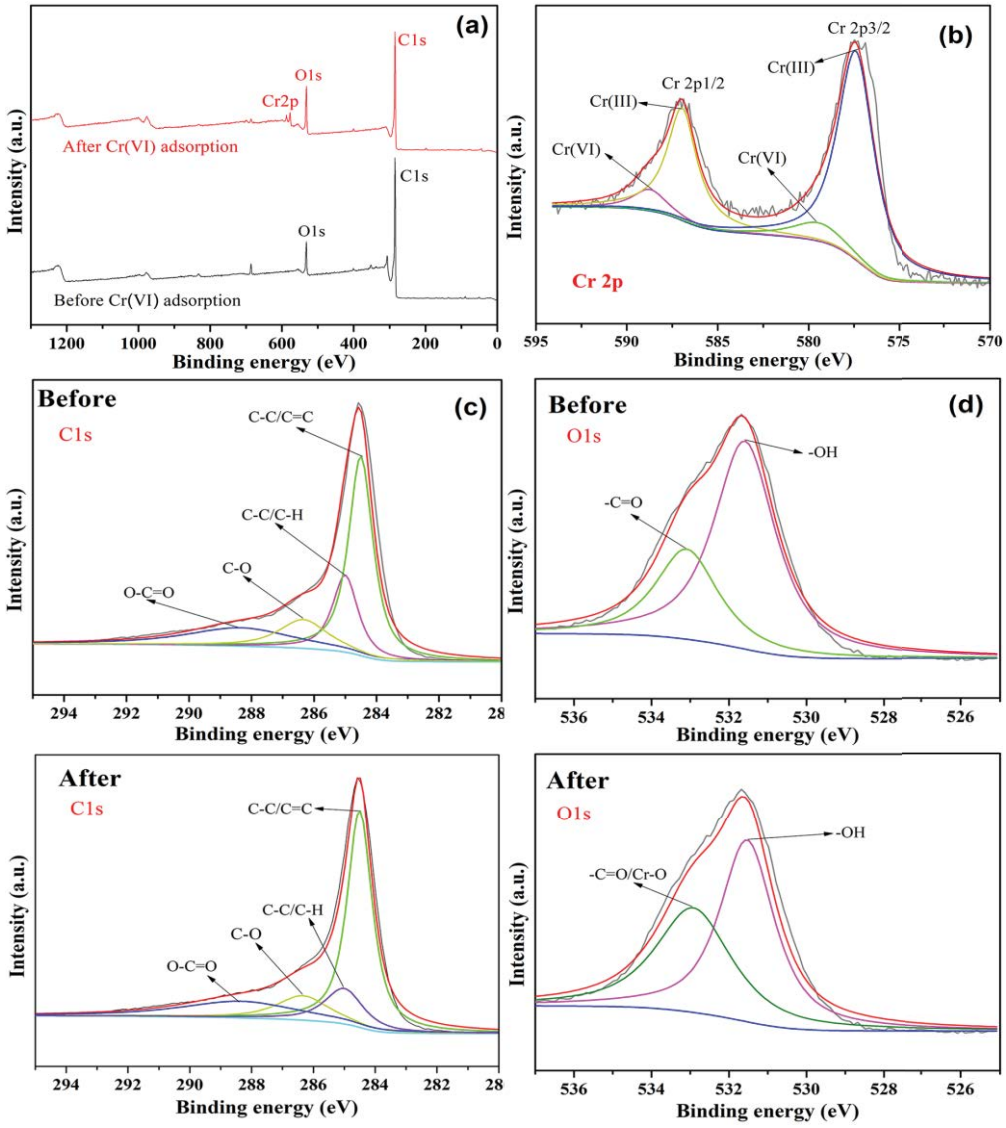

Fig. 9. X-ray photoelectron spectra of (a) fresh and used AC-800, (b) Cr2p spectra of used AC-800, (c) C1s spectra of used AC-800 and (d) O1s spectra of used AC-800.

indicates the existence of intraparticle diffusion in the Cr(VI) adsorption process.

4. Conclusions

In this work, KOH-activated carbon produced from *Ipomoea batatas* vine has a high specific surface area and abundant pore structure, which could efficiently remove Cr(VI) from an aqueous solution. The activated carbon prepared at 800°C shows a maximum adsorption capacity as high as 362.3 mg/g. According to the results of characterization, pyrolysis temperature significantly affects the surface structure and the specific surface area of the activated carbon. The analysis of FTIR and XPS revealed that the removal process of Cr(VI) by activated carbon not only exists physisorption, but also chemisorption where Cr(VI) would be reduced to Cr(III) by activated carbon and precipitate on the surface of activated carbon by complexation. The adsorption of Cr(VI) onto activated carbon agreed well with the pseudo-second-order kinetic and Langmuir adsorption model, demonstrating that the adsorption process was monolayer chemisorption. The Cr(VI) removal was highly pH-dependent and higher removal rate at lower initial pH. With these results, *Ipomoea batatas* vine could be used as a promising precursor to produce activated carbon, with considerable potential to remove Cr(VI) from wastewater.

Acknowledgements

This work was supported by The University Synergy Innovation Program of Anhui Province (GXXT-2020-075) and The Anhui Laboratory of Molecule-Based Materials (fzj21008).

Declaration of interests

The authors declare that they have no known competing financial interests or personal relationships that could have appeared to influence the work reported in this paper.

References

[1] T. Wang, D. Sun, Q. Zhang, Z.Z. Zhang, China's drinking water sanitation from 2007 to 2018: a systematic review, Sci. Total Environ., 757 (2021) 143923, doi: 10.1016/j.scitotenv.2020.143923.
[2] D. Ayhan, Heavy metal adsorption onto agro-based waste materials: a review, J. Hazard. Mater., 157 (2008) 202–229.
[3] L. Niazi, A. Lashanizadegan, H. Sharififard, Chestnut oak shells activated carbon: preparation, characterization and application for Cr(VI) removal from dilute aqueous solutions, J. Cleaner Prod., 185 (2018) 554–561.
[4] V.K. Gupta, I. Ali, T.A. Saleh, M. Siddiqui, S. Agarwal, Chromium removal from water by activated carbon developed from waste rubber tires, Sustainable Chem. Pharm., 7 (2013) 9–16.
[5] S. Sangkarak, A. Phetrak, S. Kittipongvises, D. Kitkaew, D. Phihusut, J. Lohwacharin, Adsorptive performance of activated carbon reused from household drinking water filter for hexavalent chromium-contaminated water, J. Environ. Manage., 272 (2020) 111085, doi: 10.1016/j.jenvman.2020.111085.
[6] L. Me, C. Amrhein, F. Wt, Environmental biochemistry of chromium, Rev. Environ. Contam. Toxicol., 136 (1994) 91–121.
[7] J.M. Zhao, L.H. Yu, H.X. Ma, F. Zhou, K.Y. Yang, G. Wu, Corn stalk-based activated carbon synthesized by a novel activation method for high-performance adsorption of hexavalent chromium in aqueous solutions, J. Colloid Interface Sci., 578 (2020) 650–659.
[8] M. Erdem, H.S. Altundogan, M.D. Turan, F. Tumen, Hexavalent chromium removal by ferrochromium slag, J. Hazard. Mater., 126 (2005) 176–182.
[9] l. Gzara, M. Dhahbi, Removal of chromate anions by micellar-enhanced ultrafiltration using cationic surfactants, Desalination, 137 (2001) 241–250.
[10] Y.Q. Xie, J. Lin, J. Liang, M. Li, Y. Fu, H.T. Wang, T. Song, J. Li, Hypercrosslinked mesoporous poly(ionic liquid)s with high density of ion pairs: efficient adsorbents for Cr(VI) removal via ion-exchange, Chem. Eng. J., 378 (2019) 122107, doi: 10.1016/j.cej.2019.122107.
[11] S.S. Li, F. Yang, J.S. Li, K. Cheng, Porous biochar-nanoscale zero-valent iron composites: synthesis, characterization and application for lead ion removal, Sci. Total Environ., 746 (2020) 141037, doi: 10.1016/j.scitotenv.2020.141037.
[12] K. Lu, T.T. Wang, Z. Li, S.P. Dong, S.X. Gao, L. Mao, Adsorption behavior and mechanism of Fe–Mn binary oxide nanoparticles: adsorption of methylene blue, J. Colloid Interface Sci., 539 (2019) 553–562.
[13] S. Urmetzer, J. Lask, R. Vargas-Carpintero, A. Pyka, Learning to change: transformative knowledge for building a sustainable bioeconomy, Ecol. Econ., 167 (2020) 106435, doi: 10.1016/j.ecolecon.2019.106435.
[14] J. Ru, X.M. Wang, F.B. Wang, X.L. Cui, X.Z. Du, X.Q. Lu, UiO series of metal-organic frameworks composites as advanced sorbents for the removal of heavy metal ions: synthesis, applications and adsorption mechanism, Ecotoxicol. Environ. Saf., 208 (2021) 111577, doi: 10.1016/j.ecoenv.2020.111577.
[15] F.L. Kong, Y. Zhang, H.S. Wang, J.G. Tang, Y. Li, S. Wang, Removal of Cr(VI) from wastewater by artificial zeolite spheres loaded with nano Fe–Al bimetallic oxide in constructed wetland, Chemosphere, 257 (2020) 127224, doi: 10.1016/j.chemosphere.2020.127224.
[16] J.A.R. Willemsen, I.C. Bourg, Molecular dynamics simulation of the adsorption of per-and polyfluoroalkyl substances (PFASs) on smectite clay, J. Colloid Interface Sci., 585 (2021) 337–346.
[17] X.H. Qi, L.Y. Li, Y. Wang, N. Liu, R.L. Smith Jr., Removal of hydrophilic ionic liquids from aqueous solutions by adsorption onto high surface area oxygenated carbonaceous material, Chem. Eng. J., 256 (2014) 407–414.
[18] X.F. Chen, X.W. Peng, X.Q. Ma, Investigation of Mannich reaction during co-liquefaction of microalgae and sweet potato waste: combustion performance of bio-oil and bio-char, Bioresour. Technol., 317 (2020) 123993, doi: 10.1016/j.biortech.2020.123993.
[19] K. Azizi, K.M. Moraveji, H.A. Najafabadi, Characteristics and kinetics study of simultaneous pyrolysis of microalgae *Chlorella vulgaris*, wood and polypropylene through TGA, Bioresour. Technol., 243 (2017) 481–491.
[20] A.C.K. Klinger, L.P. da Silva, G.S.P. de Toledo, D.B. Falcone, F.R. Goulart, Sweet potato vines in diets for growing rabbits on performance, carcass characteristics and meat quality, Anim. Sci. J., 89 (2018) 1556–1560.
[21] S.J. Chen, S.S. Tang, Y. Sun, G. Wang, H. Chen, X.X. Yu, Y.J. Su, G. Chen, Preparation of a highly porous carbon material based on quinoa husk and its application for removal of dyes by adsorption, Materials, 11 (2018) 1407, doi: 10.3390/ma11081407.
[22] H.Z. Qiao, H.M. Shao, X.J. Zheng, J.W. Liu, J.Q. Liu, J. Huang, C.Y. Zhang, Z. Liu, J.R. Wang, W.T. Guan, Modification of sweet potato (*Ipomoea batatas* Lam.) residues soluble dietary fiber following twin-screw extrusion, Food Chem., 335 (2021) 127522, doi: 10.1016/j.foodchem.2020.127522.
[23] X.F. Chen, X.W. Peng, X.Q. Ma, J.J. Wang, Investigation of Mannich reaction during co-liquefaction of microalgae and sweet potato waste, Bioresour. Technol., 284 (2019) 286–292.
[24] J.-L. Li, Z.-X. Deng, X.-H. Ji, X.-G. Luo, Absorption and interaction mechanisms of uranium & cadmium in purple sweet potato (*Ipomoea batatas* L.), J. Hazard. Mater., 400 (2020) 123264, doi: 10.1016/j.jhazmat.2020.123264.
[25] B.Y. Tu, R.T. Wen, K.Q. Wang, Y.L. Cheng, Y.Q. Deng, W. Cao, K.H. Zhang, H.S. Tao, Efficient removal of aqueous hexavalent

chromium by activated carbon derived from Bermuda grass, J. Colloid Interface Sci., 560 (2019) 649–658.
[26] N. Leila, L. Asghar, S. Hakimeh, Chestnut oak shells activated carbon: preparation, characterization and application for Cr(VI) removal from dilute aqueous solutions, J. Clean. Prod., 185 (2018) 554–561.
[27] S. Sirirat, P. Athit, K. Suthirat, K. Duangta, P. Doungkamon, L. Jenyuk, Adsorptive performance of activated carbon reused from household drinking water filter for hexavalent chromium-contaminated water, J. Environ. Manage., 272 (2020) 111085.
[28] V.K. Gupta, I. ALI, T.A. Saleh, M. Siddiqui, S. Agarwal, Activated porous carbon materials with ultrahigh specific surface area derived from banana peels for high-performance lithium-sulfur batteries, J. Mater. Sci-Mater El., 29 (2013) 11325–11335.
[29] Y.H. Cao, K.L. Wang, X.M. Wang, Z.R. Gu, Q.H. Fan, W. Gibbons, J.D. Hoefelmeyer, P.R. Kharel, M. Shrestha, Hierarchical porous activated carbon for supercapacitor derived from corn stalk core by potassium hydroxide activation, Electrochimica. Acta., 212 (2016) 839–847.
[30] H. Sharififard, F. Pepe, M. Soleimani, P. Aprea, D. Caputo, Iron-activated carbon nanocomposite: synthesis, characterization and application for lead removal from aqueous solution, RSC Adv., 6 (2016) 1395–1403.
[31] G.A. Adebisi, Z.Z. Chowdhury, P.A. Alaba, Equilibrium, kinetic, and thermodynamic studies of lead ion and zinc ion adsorption from aqueous solution onto activated carbon prepared from palm oil mill effluent, J. Cleaner Prod., 148 (2017) 958–968.
[32] Q.Y. Zhou, X. Jiang, X. Li, C.Q. Jia, W.J. Jiang, Preparation of high-yield N-doped biochar from nitrogen-containing phosphate and its effective adsorption for toluene, RSC Adv., 8 (2018) 30171–30179.
[33] J.W. Jin, Y.N. Li, Y.Z. Zhang, S.C. Wu, Y.C. Cao, P. Liang, J. Zhang, M.H. Wong, M.Y. Wang, S.D. Shan, P. Christie, Influence of pyrolysis temperature on properties and environmental safety of heavy metals in biochars derived from municipal sewage sludge, J. Hazard. Mater., 320 (2016) 417–426.
[34] L. Niazi, A. Lashanizadegan, H. Sharififard, Chestnut oak shells activated carbon: preparation, characterization and application for Cr(VI) removal from dilute aqueous solutions, J. Cleaner Prod., 185 (2018) 554–561.
[35] S. Yang, S.L. Wang, X. Liu, L. Li, Biomass derived inter-connected hierarchical micro-meso-macro-porous carbon with ultrahigh capacitance for supercapacitors, Carbon, 147 (2019) 540–549.
[36] J. Cheng, J.-J. Gu, W. Tao, P. Wang, L. Liu, C.-Y. Wang, Y.-K. Li, X.-H. Feng, G.-H. Qiu, F.-F. Cao, Edible fungus slag derived nitrogen-doped hierarchical porous carbon as a high-performance adsorbent for rapid removal of organic pollutants from water, Bioresour. Technol., 294 (2019) 122149, doi: 10.1016/j.biortech.2019.122149.
[37] H. Sharififard, M. Aoleimani, F. Zokaee, Evaluation of activated carbon and bio-polymer modified activated carbon performance for palladium and platinum removal, J. Taiwan Inst. Chem. Eng., 43 (2012) 696–703.
[38] M.X. Chen, F.F. He, D.W. Hu, C.Z. Bao, Q. Huang, Broadened operating pH range for adsorption/reduction of aqueous Cr(VI) using biochar from directly treated jute (*Corchorus capsularis* L.) fibers by H_3PO_4, Chem. Eng. J., 381 (2020) 122739, doi: 10.1016/j.cej.2019.122739.
[39] Z.T. Zeng, S.J. Ye, H.P. Wu, R. Xiao, G.M. Zeng, J. Liang, C. Zhang, J.F. Yu, Y.L. Fang, B. Song, Research on the sustainable efficacy of g-MoS_2 decorated biochar nanocomposites for removing tetracycline hydrochloride from antibiotic-polluted aqueous solution, Sci. Total Environ., 648 (2018) 206–217.
[40] M.K. Amosa, M.S. Jami, M.F.R. Alkhatib, Electrostatic biosorption of COD, Mn and H_2S on EFB-based activated carbon produced through steam pyrolysis: an analysis based on surface chemistry, equilibria and kinetics, Waste Biomass Valorization, 7 (2016) 109–124.
[41] W.J. Weber, J.C. Morris, Equilibria and capacities for adsorption on carbon, J. Sanit. Eng. Div., 90 (1964) 79–107.
[42] X. Zhang, W.J. Fu, Y.X. Yin, Z.H. Chen, R.L. Qiu, M.-O. Simonnot, X.F. Wang, Adsorption-reduction removal of Cr(VI) by tobacco petiole pyrolytic biochar: batch experiment, kinetic and mechanism studies, Bioresour. Technol., 268 (2018) 149–157.
[43] J.H. Qu, S.Q. Wang, L.Y. Jin, Y. Liu, R.L. Yin, Z. Jiang, Y. Tao, J.J. Huang, Y. Zhang, Magnetic porous biochar with high specific surface area derived from microwave-assisted hydrothermal and pyrolysis treatments of water hyacinth for Cr(VI) and tetracycline adsorption from water, Bioresour. Technol., 340 (2021) 125692, doi: 10.1016/j.biortech.2021.125692.
[44] B.Y. Tu, R.T. Wen, K.Q. Wang, Y.L. Cheng, Efficient removal of aqueous hexavalent chromium by activated carbon derived from Bermuda grass, J. Colloid Interface Sci., 560 (2020) 649–658.
[45] X. Zhang, L. Zhang, A. Li, Eucalyptus sawdust derived biochar generated by combining the hydrothermal carbonization and low concentration KOH modification for hexavalent chromium removal, J. Environ. Manage., 206 (2018) 989–998.
[46] H. Demiral, I. Demiral, F. Tümsek, B. Karabacakoğlu, Adsorption of chromium(VI) from aqueous solution by activated carbon derived from olive bagasse and applicability of different adsorption models, Chem. Eng. J., 144 (2008) 188–196.
[47] J.X. Wu, X.L. Yan, L. Li, J.H. Gu, T. Zhang, L.L. Tian, X.T. Su, Z. Lin, High-efficiency adsorption of Cr(VI) and RhB by hierarchical porous carbon prepared from coal gangue, Chemosphere, 275 (2021) 130008, doi: 10.1016/j.chemosphere.2021.130008.
[48] Z. Sun, B. Liu, M. Li, C. Li, S. Zheng, Carboxyl-rich carbon nanocomposite based on natural diatomite as adsorbent for efficient removal of Cr(VI), J. Mater. Res. Technol., 9 (2019) 948–959.
[49] J. Yang, M. Yu, W. Chen, Adsorption of hexavalent chromium from aqueous solution by activated carbon prepared from longan seed: kinetics, equilibrium and thermodynamics, J. Ind. Eng. Chem., 21 (2015) 414–422.
[50] N.H. Kera, M. Bhaumik, K. Pillay, S.S. Ray, A. Maity, Selective removal of toxic Cr(VI) from aqueous solution by adsorption combined with reduction at a magnetic nanocomposite surface, J. Colloid Interface Sci., 503 (2017) 214–228.
[51] M. Mahapatra, M. Karmakar, A. Dutta, H. Mondal, J.S.D. Roy, P. Chattopadhyay, N. Ranjan Singha, Microstructural analyses of loaded and/or unloaded semisynthetic porous material for understanding of super adsorption and optimization by response surface methodology, J. Environ. Chem. Eng., 6 (2018) 289–310.
[52] M.B. Wu, Y. Wang, W.T. Wu, C. Hu, X.N. Wang, J.T. Zheng, Z.T. Li, B. Jiang, J.S. Qiu, Preparation of functionalized water-soluble photoluminescent carbon quantum dots from petroleum coke, Carbon, 78 (2014) 480–489.
[53] Z. Yue, S.E. Bender, J.W. Wang, J. Economy, Removal of chromium Cr(VI) by low-cost chemically activated carbon materials from water, J. Hazard. Mater., 166 (2009) 74–78.
[54] Y.-J. Shih, C.-D. Dong, Y.-H. Huang, C.P. Huang, Electro-sorption of ammonium ion onto nickel foam supported highly microporous activated carbon prepared from agricultural residues (dried *Luffa cylindrica*), Sci. Total Environ., 673 (2007) 296–305.
[55] M. Su, Y.L. Fang, B. Li, W.Z. Yin, J.J. Gu, H. Liang, P. Li, J.H. Wu, Enhanced hexavalent chromium removal by activated carbon modified with micro-sized goethite using a facile impregnation method, Sci. Total Environ., 647 (2019) 47–56.
[56] V.K. Gupta, I. Ali, T.A. Saleh, M. Siddiqui, S. Agarwal, Activated porous carbon materials with ultrahigh specific surface area derived from banana peels for high-performance lithium-sulfur batteries, J. Mater. Sci.: Mater. Electron., 29 (2013) 11325–11335.

Supporting information

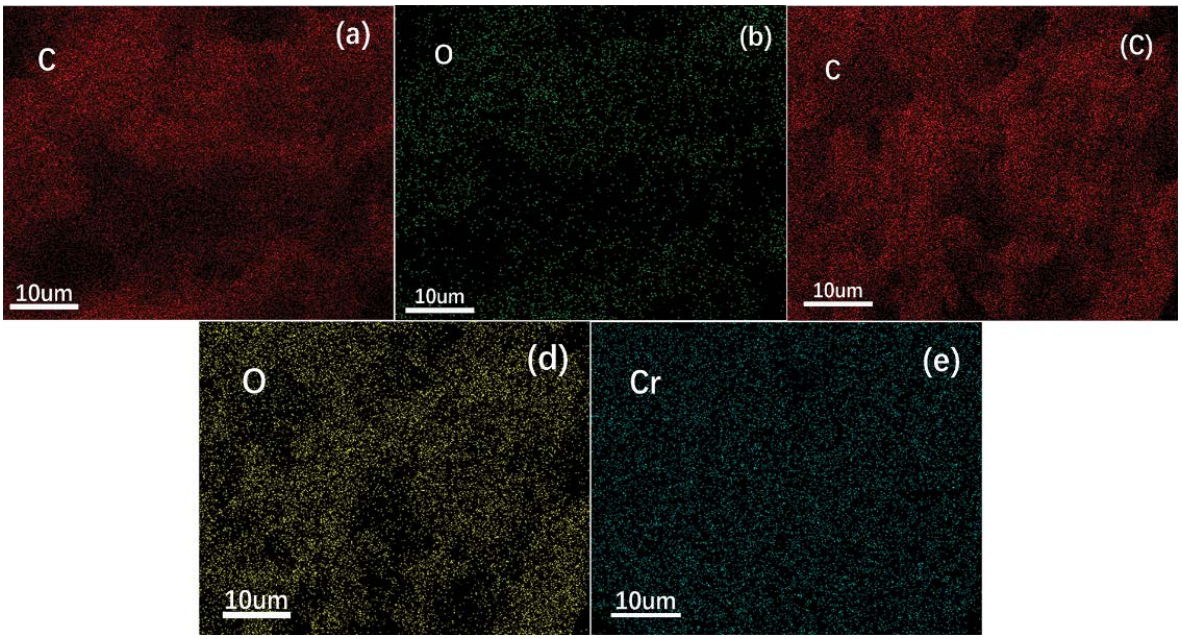

Fig. S1. Mapping images of AC-800 before and after Cr(VI) adsorption.

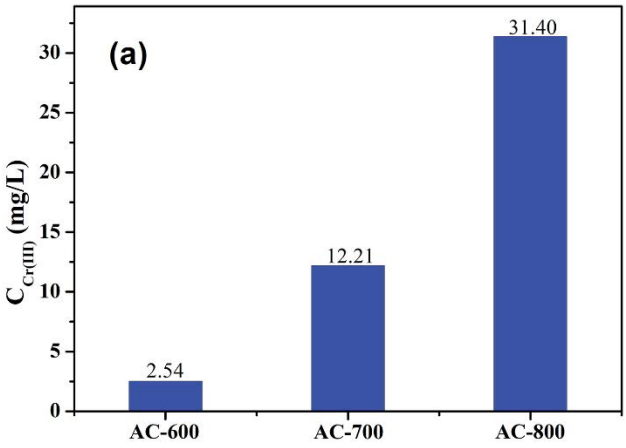

Fig. S2. Concentration of Cr(III) in remained solution (pH = 2).

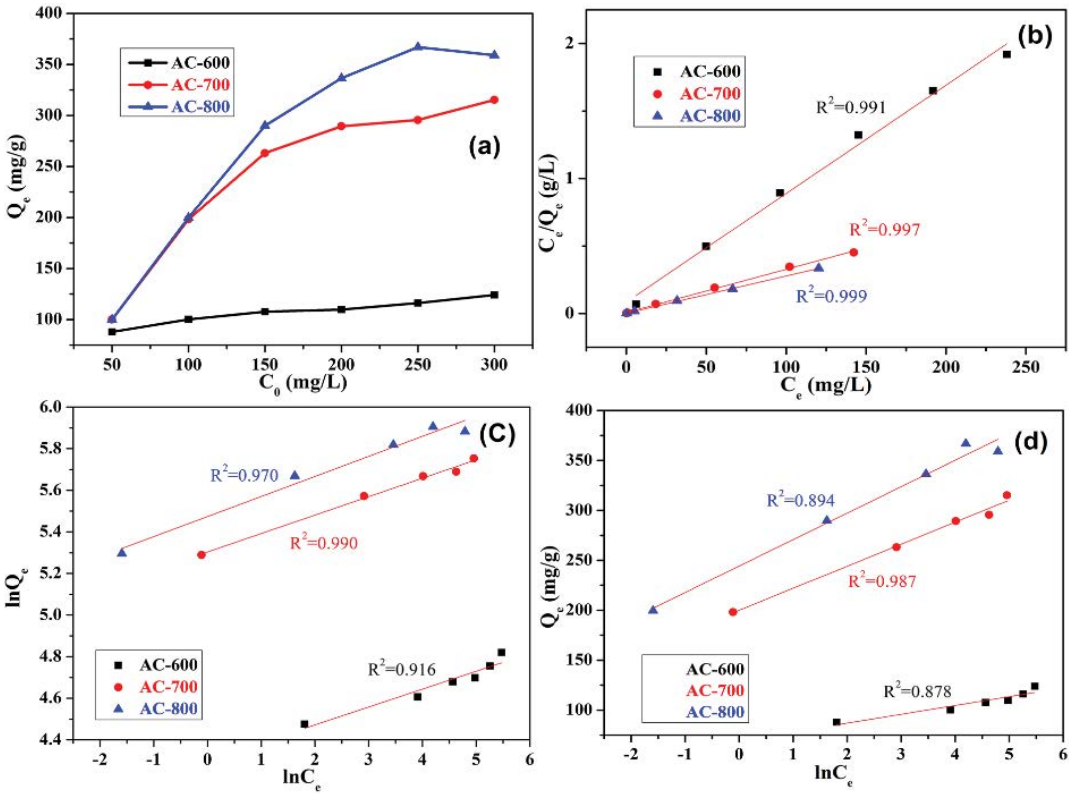

Fig. S3. (a) Adsorption isotherm of Cr(VI) onto the activated carbons and (b) Langmuir isotherm model, (c) Freundlich isotherm model, and Temkin isotherm model.